Chapter 3

Effects of Implant Damage Above the Amorphization Threshold

3.1 Introduction

As device dimensions have shrunk into the submicron regime, the effects of ion implantation damage on dopant diffusion have become increasingly important. Currently, dopant diffusion in many advanced technologies is predominantly controlled by the effects of implantation damage. Unfortunately, our current understanding of the interaction between implant damage and dopant diffusion is limited. For this reason, it is very difficult to predict final doping profiles even using advanced process simulation programs like SUPREM-IV. In this chapter, we first survey the current research status regarding implant-damage enhanced diffusion (IED). Then we describe the experiment we have performed in order to characterize the enhanced diffusion of a boron marker layer due to silicon implantation damage above the amorphization threshold. Finally, we characterize the quality of the epitaxially grown silicon used in our experiments by comparing inert boron diffusion in the epitaxial material to inert boron diffusion in float-zone silicon.

3.2 Previous Experiments

In the early 1980 s, there was some controversy over the mechanism by which enhanced diffusion of implanted boron occurred. One theory proposed that during the boron implant, some of the boron channeled and ended up as interstitial boron. During annealing, these interstitial boron atoms diffused large distances before coming to rest on substitutional lattice sites [36]-[38]. Then the transient enhanced diffusion (TED) of the boron would be over, and only normal, inert diffusion of the boron would be observed. Another theory proposed that point defects generated by the implant process itself were responsible for the TED of the boron [39]. Enhanced diffusion continued as long as point defects concentrations remained above their equilibrium values.

There have been numerous additional studies on boron diffusion as well as some on phosphorus diffusion which all support the theory that implant damage is responsible for the TED [9],[11],[26],[40]-[56]. These results are described below.

In a clever isotopic experiment, Cho *et al.* [40] first implanted B^{11} at an energy of 50 keV and a dose of $1x10^{15}$ cm^{-2}, then performed an RTA anneal such that the TED of the B^{11} was over. Next, another $1x10^{15}$ cm^{-2}, 50 keV B^{10} implant was done followed by another RTA. If indeed, TED is caused by the migration of channeled atoms in interstitial sites, then only the B^{10} should exhibit TED during the second RTA and the B^{11} profile should remain unchanged. If, on the other hand, implant damage causes the TED, then the B^{11} should undergo additional motion during the second RTA. The latter result was observed experimentally supporting the theory that implant damage causes TED.

Michel *et al.* [42] have done a study on boron TED as a function of anneal temperature. For identical boron implants of $2x10^{14}$ cm^{-2}, 60 keV energy, samples were annealed at temperatures from 800ßC to 1000ßC. If the channeled interstitial boron theory is correct, then the same number of boron atoms will exhibit TED regardless of the temperature since the number of channeled boron atoms on interstitial sites only depends on the implantation condition and not on the anneal temperature. However, they found experimentally that the percentage of boron that exhibits enhanced diffusion increases with increasing anneal temperature. This behavior was explained by assuming the boron

implant created point defect clusters and that these defect clusters emitted point defects during the subsequent anneals, the emission rate being larger for higher temperature anneals. This explanation is based on implant damage causing TED.

Kim *et al.* [50] performed an experiment in which BF_2 was implanted into silicon samples at $2x10^{14}$ cm^{-2}, 40 keV. Before annealing the samples, the top 800 of the samples was chemically etched off. After RTA at 900ßC for 30 seconds in a nitrogen ambient, the boron profiles were measured with SIMS. The boron did not exhibit any enhanced diffusion indicating that implant damage in the surface region causes TED.

Finally, there have been numerous studies in which the starting material contains completely stabilized, substitutional boron or phosphorus profiles [1],[3],[11],[41],[43]-[46],[48],[49],[53],[55],[56]. Silicon is then implanted in the surface region, and, after furnace annealing or RTA, enhanced diffusion of both boron and phosphorus has been observed indicating that TED is due to damage from the silicon implant. If TED was due to channeled interstitial atoms moving large distances, no enhanced diffusion would have been observed after the silicon implant since all the dopant is already sitting on substitutional sites (except for the atoms that account for normal inert diffusion).

In summary, although there was initially some controversy as to the mechanism that causes TED of boron and phosphorus, the majority of current experimental data strongly indicates that implant damage causes TED.

In our work, we investigate the effects of implantation damage above the amorphization threshold on dopant diffusion. Before presenting our experimental work, it is useful to look at the work that has already been done on implantation damage both below and above the amorphization threshold.

3.2.1 Implant Damage Below the Amorphization Threshold

Packan [1],[11] has done an extensive experimental study of the TED of a low-concentration, deep-implanted boron marker layer after ^{29}Si implants and subsequent furnace anneals at temperatures between 750ßC and 1000ßC. In his experiments, the boron was implanted and then annealed at 900ßC for 10 minutes to ensure that the implanted boron sits on substitutional sites and that the TED due to the self-implant is completely

annealed out. Using these samples as the starting condition, Packan then studied the TED as a function of ^{29}Si implant dose and energy, as well as final anneal time and temperature. We summarize the major findings of his study.

3.2.1.1 Effect of Implant Dose

The enhanced diffusion of the boron marker layer increases as the implant dose increases. However, doubling the silicon implant dose does not double the enhanced diffusion of the boron. The increase in enhanced diffusion is sublinear with silicon implant dose.

3.2.1.2 Effect of Implant Energy

For very low implant energies (10 keV to 40 keV), the enhanced diffusion increased rapidly with increasing implant energy for all temperatures investigated. However, for higher temperature anneals (900ßC and 1000ßC), only small increases in the enhanced diffusion of boron was observed for 40, 80, and 200 keV implants. This small increase in enhanced diffusion with increasing implant energy is similar to the results seen by Miyake and Aoyama [47]. Implantation at higher energies changes the implant damage distribution. For a constant dose implant, a higher energy will place the damage deeper into the substrate, spread the damage over a larger volume, and reduce the peak value of damage. Furthermore, the effects of surface recombination, bulk recombination, and the generation of extended defects can all change with varying implant energy. Although no current physical theory can quantitatively predict this energy dependence of enhanced diffusion, it has been modeled empirically in [23] where the maximum enhanced diffusion depends logarithmically on the implant energy.

3.2.1.3 Time-Dependence

For very short anneal times, the enhanced diffusion of the boron marker layer was independent of the silicon implant dose indicating a saturation effect in the enhanced diffusion. However, for long anneal times such that TED was complete, samples implanted with higher silicon doses did have broader final profiles. This is simply because

point defect concentrations remain above equilibrium for a longer time after higher dose silicon implants.

3.2.1.4 Temperature-Dependence

For identical silicon implant conditions, the enhanced diffusion of the marker layer was larger for lower temperatures as observed by others [2],[3],[41],[42],[47],[49]. In addition, the transient of the enhanced diffusion was longer for lower temperature anneals. These two effects are easily explained. The enhanced diffusion is larger at lower temperatures simply because equilibrium point defect concentrations are lower at lower temperatures, and thus point defect supersaturations are larger at lower temperatures. The TED lasts longer at lower temperatures because diffusion and recombination processes of the implant-generated point defects are slower at lower temperatures. The combination of these two effects can result in final boron profiles that are broader for samples annealed at lower temperatures. RTA is an attractive alternative to standard furnace annealing for limiting TED because the high-temperature, short-time RTA results in less enhanced diffusion as well as shorter transients for the enhanced diffusion. However, RTA anneals are typically done at high temperatures resulting in larger inert diffusivites as compared to low-temperature furnace anneals. Thus ultimately there is a trade-off between limiting the effects of implant damage versus limiting the amount of inert diffusion regardless of whether an RTA or furnace anneal is used.

3.2.2 Implant Damage Above the Amorphization Threshold

There have also been numerous studies of implant damage above the amorphization threshold via self-implant or silicon implant [9],[10],[26],[41],[44]-[46],[48],[49],[53]. Unfortunately, these studies are not as detailed as Packan s experiments on the effects of sub-amorphization damage on boron diffusion. However, in general, the results from these high-dose experiments are that whether or not enhanced diffusion is observed depends on the location of the dopant with respect to the depth of the amorphous layer. For boron and phosphorus located beyond the amorphous layer, TED is still observed while for boron

and phosphorus located within the amorphous layer, inert diffusion, or at least much less TED, is observed.

Unfortunately, in all of these studies, the direct interpretation of the effect of implant damage above the amorphization threshold on dopant diffusion is very difficult because of the multiple physical phenomena that contribute to the final doping profile. Typically, implant doses are high enough such that the silicon is doped extrinsically at the anneal temperature. At very high doping levels, dopant solid solubility becomes important as dopants begin to form either precipitates or clusters [57]. Overlap of the dopant and the damaged region can lead to direct interaction between the dopant and the defects generated from the implant. Since some regions of the substrate will contain damage below the amorphization threshold, the effects of low-dose implantation damage still play a role. All of these effects plus the role of high-dose implantation damage contribute to the final doping profile. Thus it is difficult to isolate just what role high-dose implantation damage has on dopant diffusion. We have developed an experimental test structure that eliminates all the other effects except for the low-dose and high-dose implantation damage. We have extended Packan s work in order to characterize the effects of implant damage above the amorphization threshold as a function of implant dose, implant energy, anneal time, and anneal temperature.

3.3 Experimental Procedure

Figure 3.1 shows the final structure used in this experiment. The starting material was 4-inch 0.25-0.34 Ω-cm CZ, 5-10 Ω-cm CZ, or 5.3-6.1 Ω-cm FZ, <100>, n-type silicon. For the 0.25-0.34 Ω-cm CZ wafers, a 60 minute, 1200ßC pretreatment was performed to reduce the effects of oxygen precipitation on dopant diffusion. A dry pad oxide was then grown which was subsequently etched. For all wafers, silicon epitaxy at 800ßC was used to grow boron marker layers approximately 0.25 µm thick with peak concentrations between 1 and $2x10^{18}$ cm^{-3}. Epitaxial growth was continued for another 0.3 to 0.65 µm to grow lightly-doped arsenic buffer layers on top of the boron marker layer. A thick, low temperature oxide was then deposited, and the wafers were patterned into large area

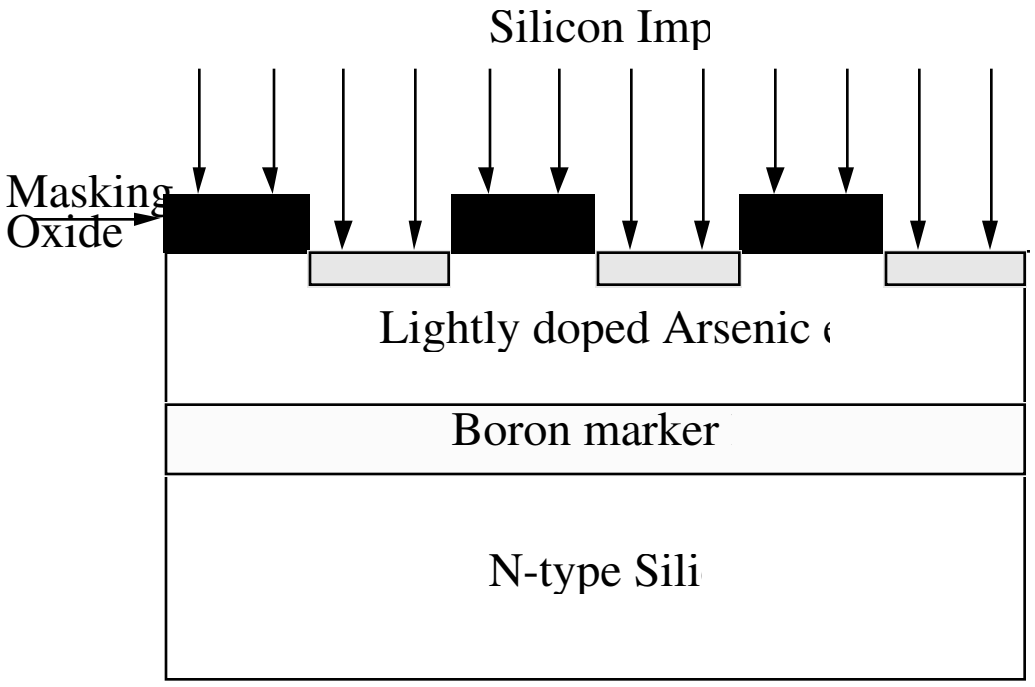

Figure 3.1 Schematic cross-section of the experimental structure used to study the effects of implantation damage below and above the amorphization threshold.

exposed and masked regions using lithography and wet etching. ^{28}Si was implanted at doses from $1x10^{14}$ cm^{-2} to $1x10^{16}$ cm^{-2} and energies between 50 and 100 keV to create the implant damage. For all samples, the beam current during silicon implantation was limited to less than 300 μA. The implant doses and energies chosen span the regime from below amorphization to above amorphization. The existence of amorphous layers as well as the depth of amorphous layers was determined via channeling RBS measurements. Another low temperature oxide was deposited as a cap layer before the wafers were furnace annealed at 750, 800, or 850ßC in an argon ambient for various times. In addition, the final anneal for one sample was an RTA at 745ßC for 2 minutes, and another sample was preannealed at 550ßC for 30 minutes before the final furnace anneal. Bevel and stain measurements were used to delineate p-n junctions of both implanted and masked regions on some wafers. Oxides were etched using HF, and initial and final boron profiles were measured with SIMS using an oxygen primary beam in a Cameca IMS-3f or 4f system. The entire experimental matrix is given in Table 3.1 and Table 3.2.

Silicon Implant		<D>/D* (750ßC)			<D>/D* (800ßC)		
Dose (cm^{-2})	Energy (keV)	10 min.	30 min.	120 min.	5 min.	10 min.	30 min.
$1x10^{15}$	50	3405	1550	535			
$2x10^{15}$	50	3575	1630				
$4x10^{15}$	50	3495	1590	530	1380	710	255
$4x10^{15}$	50	14600[1]	1660[2]				
$1x10^{16}$	50	3980	1690	550	1330	750	285
$2x10^{15}$	100	4475	1975	835	1570	955	430

Table 3.1 Experimental matrix along with extracted time-averaged enhanced diffusivities. All of the silicon implant conditions in this table generated complete surface amorphous layers. <D> is the time-averaged boron diffusivity, and D* is the default value for inert boron diffusivity in SUPREM-IV [7]. [1]The anneal condition for this sample was actually a 745ßC, 2 min. RTA. [2]The anneal condition for this sample was actually a 550ßC, 30 min. furnace anneal followed by a 750ßC, 30 min. furnace anneal.

Silicon Implant Dose (cm^{-2})	<D>/D* (750ßC)				<D>/D* (800ßC)		<D>/D* (850ßC)
	30 min.	120 min.	210 min.	510 min.	30 min.	120 min.	30 min.
$5x10^{13}$				160		105	55
$1x10^{14}$	2250	920	560	260	380	140	62
$2x10^{14}$		950		280		150	71
$4x10^{14}$		730					
$8x10^{14}$	2180	880	440	210	380	115	63
$2x10^{15}$		880					

Table 3.2 Experimental matrix along with extracted time-averaged enhanced diffusivities. All of the silicon implants in this table were done at an energy of 80 keV. From channeling RBS measurements, the implants up to the $4x10^{14}$ cm^{-2} dose were below amorphization while $8x10^{14}$ cm^{-2} and $2X10^{15}$ cm^{-2} were above amorphization. <D> is the time-averaged boron diffusivity, and D* is the default value for inert boron diffusivity in SUPREM-IV [7]

By using this experimental structure, we have reduced all the other factors discussed in the previous section except for the effect of low and high-dose implantation damage on dopant diffusion. The peak of the boron concentration is kept low to minimize the effects of high-concentration diffusion. The intrinsic carrier concentration at 750ßC is approximately $1x10^{18}$ cm^{-3} [58], such that at all temperatures studied, the material is intrinsic or only slightly extrinsic. These low concentrations also avoid boron precipitation or clustering that are normally attributed to extremely high doping levels. By growing the additional lightly-doped arsenic layer, we have physically separated the amorphous region from the boron marker layer. Regrowth of the amorphous layer and the extended defects that form at the amorphous silicon/crystalline silicon interface will not directly interact with the boron.

3.4 Experimental Results and Discussion

3.4.1 Channeling RBS Measurements

Channeling RBS measurements using 2.2 MeV He^{+} ions was performed on all the as-implanted samples. Figure 3.2 and Figure 3.3 indicate that all the silicon implant conditions given in Table 3.1 generated surface amorphous layers. The 50 keV implants generated amorphous layers between 1100 and 1300 thick while the 100 keV implant generated an amorphous layer approximately 1750 thick. Channeling RBS measurements in Figure 3.4 and Figure 3.5 show that of the silicon implant conditions in Table 3.2, surface amorphous layers approximately 1600 thick were generated only for the $8x10^{14}$ and $2x10^{15}$ cm^{-2} samples while buried amorphous layers or no amorphous layers at all were generated for the samples implanted with doses of $4x10^{14}$ cm^{-2} and below.

3.4.2 Bevel-and-Stain Measurements

Figure 3.6 is a bevel-and-stain measurement for the $2x10^{15}$ cm^{-2}, 100 keV silicon implanted sample after annealing at 750ßC for 10 minutes. The left side of the sample is a

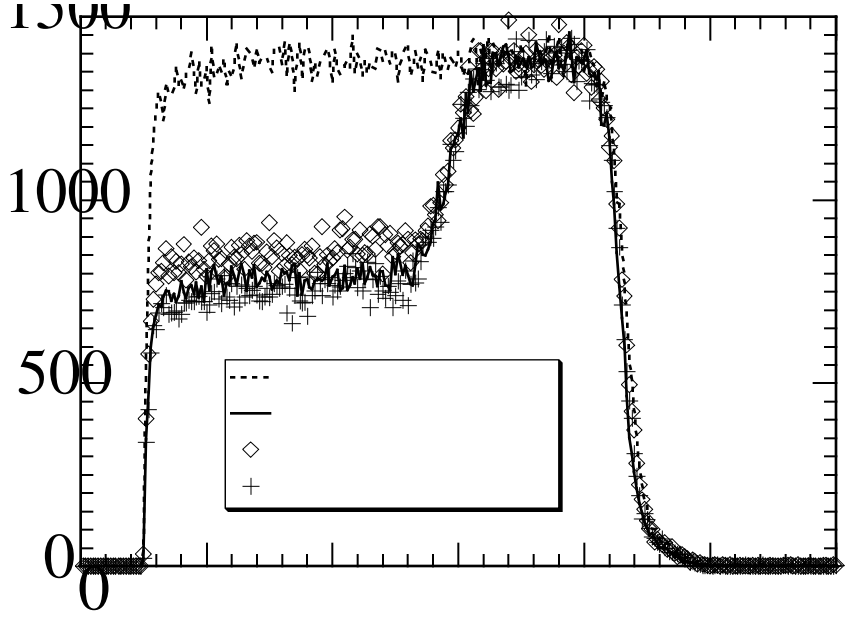

Figure 3.2 Channeling RBS measurements for the samples implanted with silicon at $1x10^{15}$, $2x10^{15}$, and $4x10^{15}$ cm^{-2} at 50 keV along with a random RBS measurement.

PostScript error

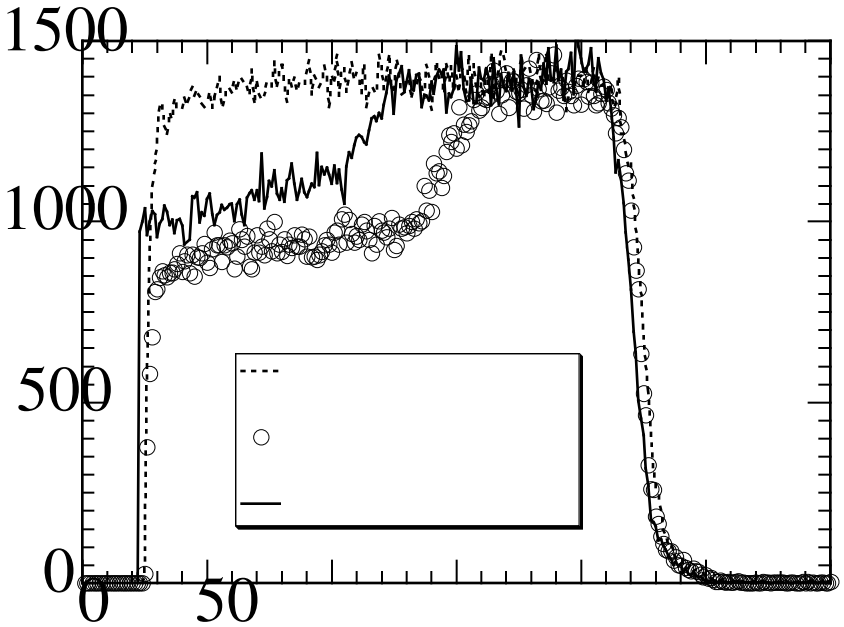

Figure 3.3 Channeling RBS measurements for the samples implanted with silicon at $1x10^{16}$ cm^{-2}, 50 keV and $2x10^{15}$ cm^{-2} at 100 keV along with a random RBS measurement.

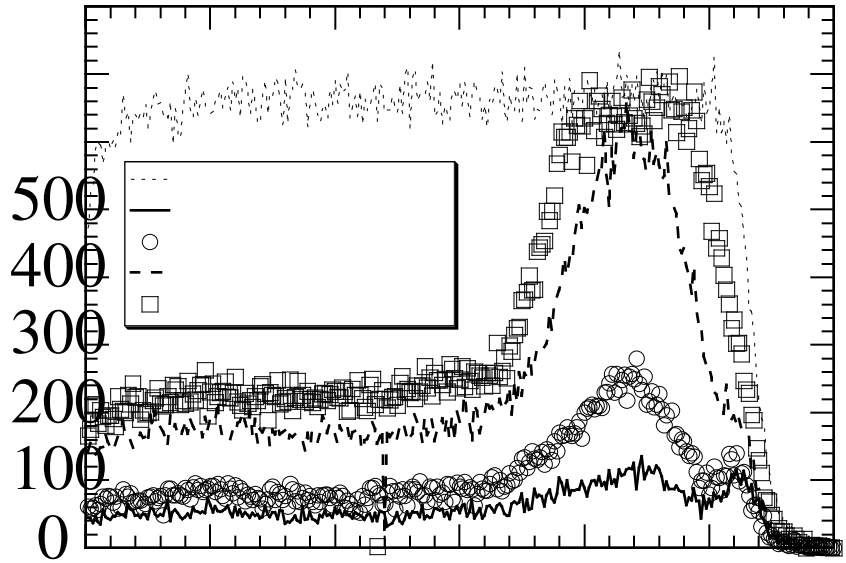

Figure 3.4 Channeling RBS measurements for the samples implanted with silicon at $1x10^{14}$, $2x10^{14}$, $4x10^{14}$ and $8x10^{14}$ cm^{-2} at 80 keV along with a random RBS measurement.

PostScript error

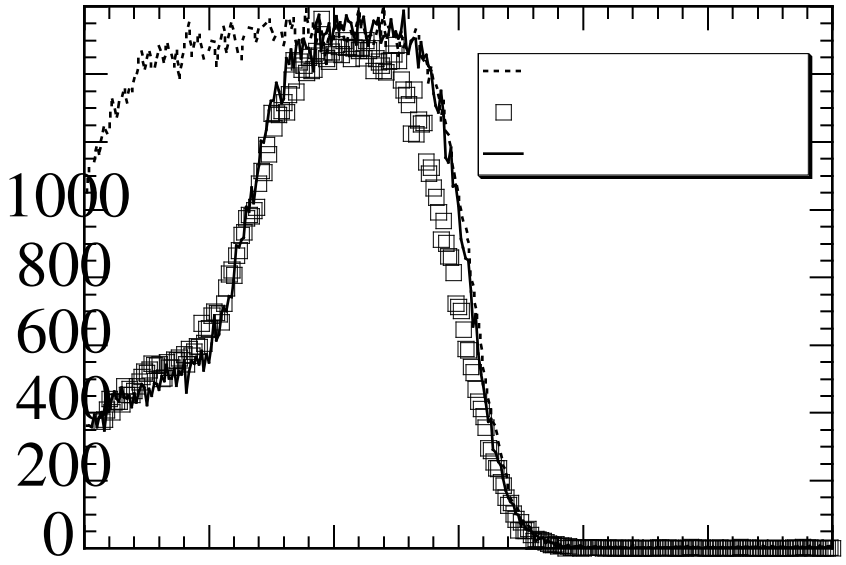

Figure 3.5 Channeling RBS measurements for the samples implanted with silicon at $8x10^{14}$ and $2x10^{15}$ cm^{-2} at 80 keV along with a random RBS measurement.

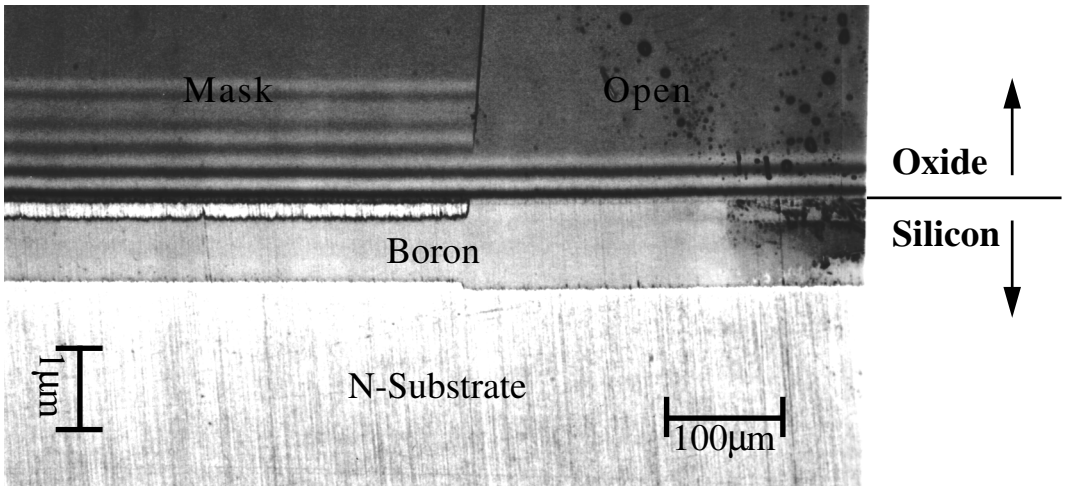

Figure 3.6 Bevel-and-stain measurement for the $2x10^{15}$ cm^{-2}, 100 keV silicon implanted sample after annealing at 750ßC for 10 minutes. The left-hand side is underneath a region masked from the silicon implant while the right-hand side is underneath an implanted region.

region that was masked from the silicon damage implant while the right side of the sample received the silicon implant. The measurement clearly shows the boron profile has diffused much more in the damaged region as compared to the masked region. Bevel-and-stain measurements on other samples showed similar results.

3.4.3 SIMS Measurements

SIMS measurements were taken on damaged regions from each sample and masked regions from the longest annealed samples at each temperature. Unannealed samples were also profiled to obtain initial boron profiles. Due to variations in the boron epilayer growth, the SIMS profiles had to be translated such that the boron peaks all coincided. Within the SIMS resolution, the data for all the masked regions showed no movement which agrees with the intrinsic boron diffusion coefficient reported by Fair [59]. Thus in all subsequent simulations, the intrinsic boron diffusivity was taken as the value from Fair which is also the default in SUPREM-IV [7]. In agreement with the bevel-and-stain measurements, the SIMS data for the damaged regions all showed much broader boron profiles compared to the initial profile.

SUPREM-IV was used to calculate time-averaged enhancements in boron diffusivity under the damaged regions. In the simulations, the initial profile was diffused into the final profiles by increasing the boron diffusion coefficient by constant multiplicative factors until the simulated profile matched the experimental SIMS data. Figure 3.7 shows the

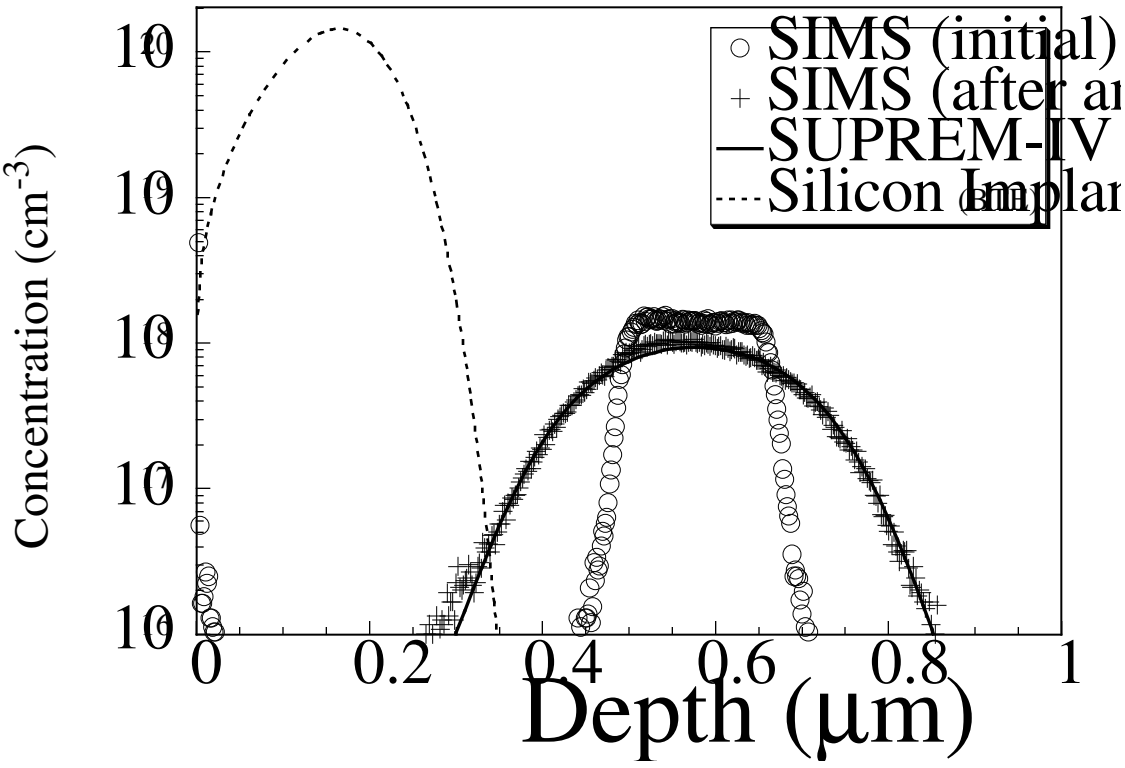

Figure 3.7 SIMS data and optimized SUPREM-IV simulation for the $2x10^{15}$ cm^{-2}, 100 keV silicon implanted, 750ßC, 30 minute annealed sample. The initial silicon implant profile (calculated using a BTE solver [27],[28]) shows the spatial separation of the implant from the diffusing layer. The enhancement in boron diffusivity for this case is 1975X.

initial SIMS boron profile, the SIMS data after a 750ßC, 30 minute anneal, and the best-fit SUPREM-IV simulation for the $2x10^{15}$ cm^{-2}, 100 keV silicon implant. Also shown in the figure is a BTE calculation [27],[28] of the initial silicon profile immediately after implant. There are several things to note from this figure. First of all, the initial boron profile is very box-shaped which gives us very good sensitivity to the effects of implantation damage. Second, there is a spatial separation of the implanted silicon profile

and the boron layer. In addition, from the channeling RBS measurements, the amorphous layers generated were less than 2000 thick. Thus, for doping concentrations within the sensitivity limit of the SIMS analysis (approximately $1x10^{16}$ cm^{-3}), there is no direct interaction between the extended defects generated by the amorphizing implant and the diffusion of the boron marker layer. Third, the boron diffuses significantly during just 30 minute annealing at 750ßC which allows easy extraction of the enhancement in boron diffusivity during the anneals. The diffusion of the boron layer is symmetric for all cases and the final profiles could be fit using simple concentration-dependent diffusivities. In fitting the data, the diffusion coefficients with neutral defects and positively charged defects were scaled by identical factors until a best-fit was obtained. The best-fit enhancements were determined via a least-squares minimization of the point-by-point difference between the SIMS data and the simulation result of the final boron profile. The extracted enhancements are summarized in Table 3.1 and Table 3.2.

3.4.3.1 Effect of Implant Dose

The main purpose of this experiment is to determine whether the enhanced diffusion of a buried boron marker layer is different for sub-amorphization implants versus amorphizing implants. There is reason to believe that the enhanced dopant diffusion will be different once one crosses the threshold for amorphization. Amorphous layer regrowth may annihilate a large fraction of the implant damage and the formation of extended defects may significantly affect the behavior of remaining point defects or point defects introduced from subsequent processing.

The dose-dependent data from Table 3.1 is plotted in Figure 3.8 and Figure 3.9 for the 750ßC and 800ßC anneals, respectively while the data for the $1x10^{14}$ cm^{-2} and the $8x10^{14}$ cm^{-2} doses from Table 3.2 is plotted in Figure 3.10 and Figure 3.11 for the 750ßC and 800ßC anneals, respectively. Recall that all the implant conditions in Figure 3.8 and Figure 3.9 amorphize the substrate. In Figure 3.10 and Figure 3.11, only the $8x10^{14}$ cm^{-2} dose generates a complete surface amorphous layer.

To first order, the enhancements in boron diffusivity are independent of the silicon implant dose, even as one crosses the amorphization threshold. This is a significant

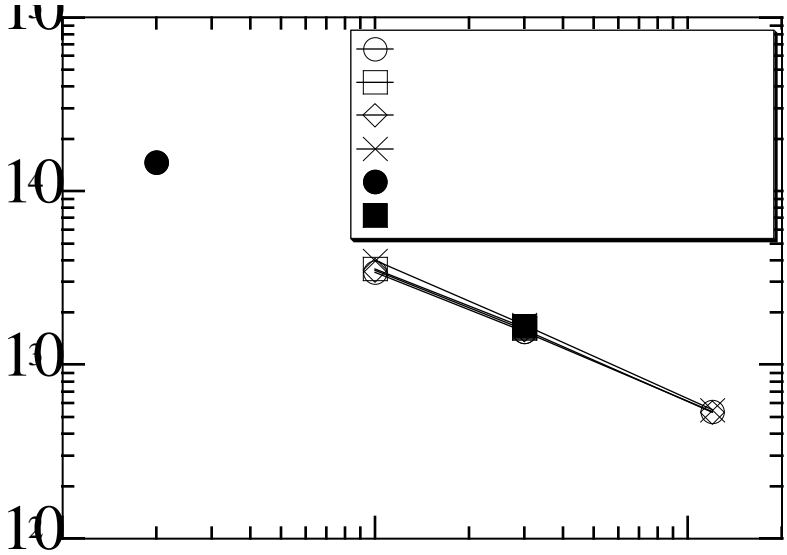

PostScript error

Figure 3.8 Extracted time-averaged boron diffusivity enhancements for various silicon implants, all above the amorphization threshold, annealed at 750ßC. The solid circle represents a $4x10^{15}$ cm^{-2} implanted sample, RTA annealed for 2 minutes at 745ßC and the solid square represents a $4x10^{15}$ cm^{-2} implanted sample preannealed at 550ßC for 30 minutes before final annealing.

experimental result indicating that inherently there is nothing special about crossing the amorphization threshold that drastically changes subsequent dopant diffusion. This conclusion is further supported by the sample preannealed at 550ßC for 30 minutes to regrow the amorphous layer. The enhanced diffusion of the boron marker layer after the additional 750ßC, 30 minute furnace anneal is identical to the enhancement measured for the sample directly annealed at 750ßC without the low temperature preanneal. Whatever physical processes occur in the original amorphous layer do not affect diffusion of the buried boron marker layer.

3.4.3.2 Effect of Implant Energy

Figure 3.12 and Figure 3.13 show the effects of silicon implant energy on the enhanced diffusion of the boron marker layer for anneals at 750ßC and 800ßC, respectively. Similar to Packan s results, our data shows that the enhanced diffusion of the

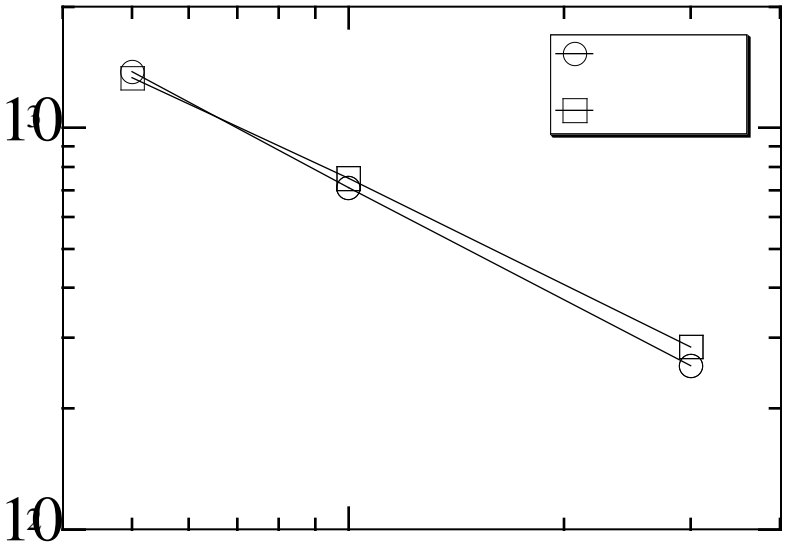

Figure 3.9 Extracted time-averaged boron diffusivity enhancements for several implant doses and energies, all above the amorphization threshold, annealed at 800ßC.

PostScript error

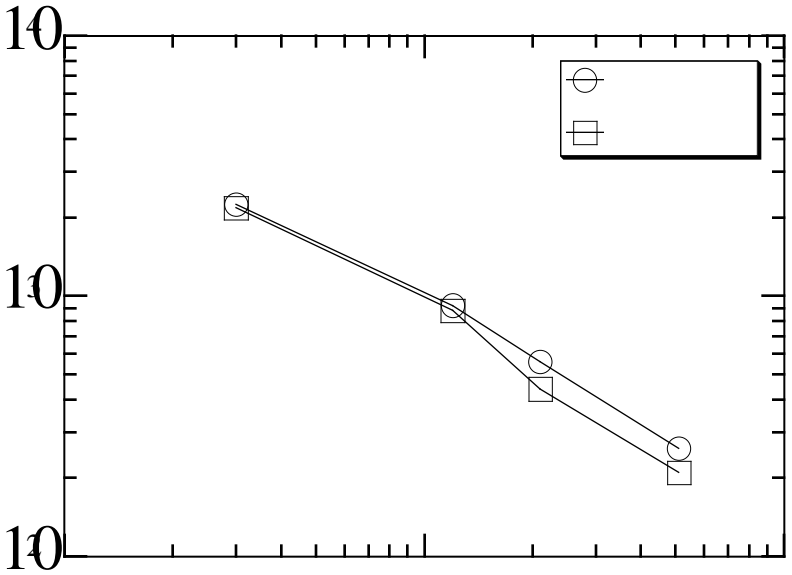

Figure 3.10 Extracted time-averaged boron diffusivity enhancements for the $1x10^{14}$ cm^{-2} (below amorphization) and the $8x10^{14}$ cm^{-2} (above amorphization) samples annealed at 750ßC for various times.

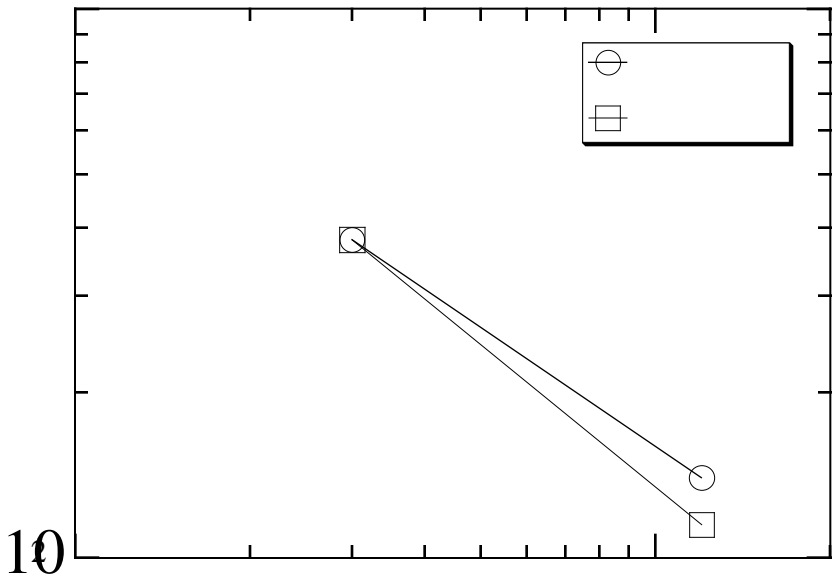

Figure 3.11 Extracted time-averaged boron diffusivity enhancements for the $1x10^{14}$ cm^{-2} (below amorphization) and the $8x10^{14}$ cm^{-2} (above amorphization) samples annealed at 800ßC for various times.

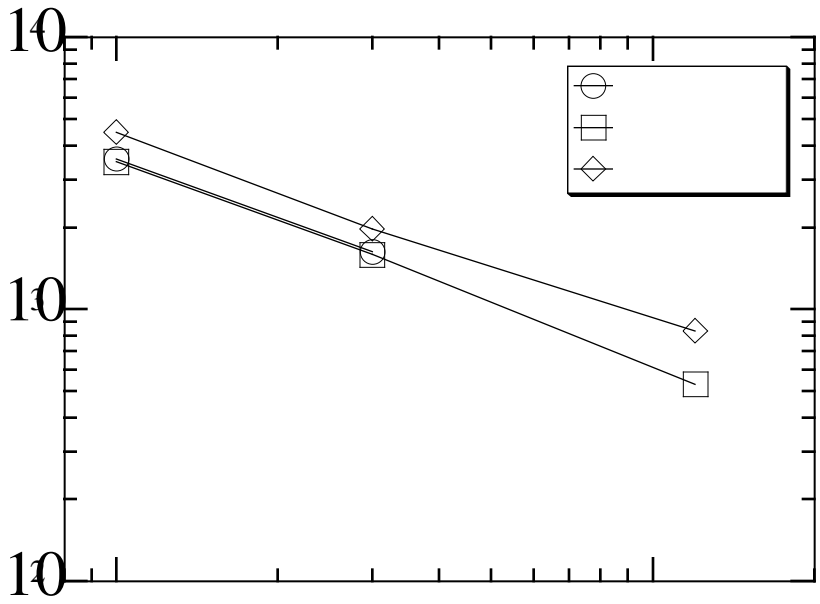

Figure 3.12 Effect of silicon implant energy on <D>/D* for the 750ßC anneals.

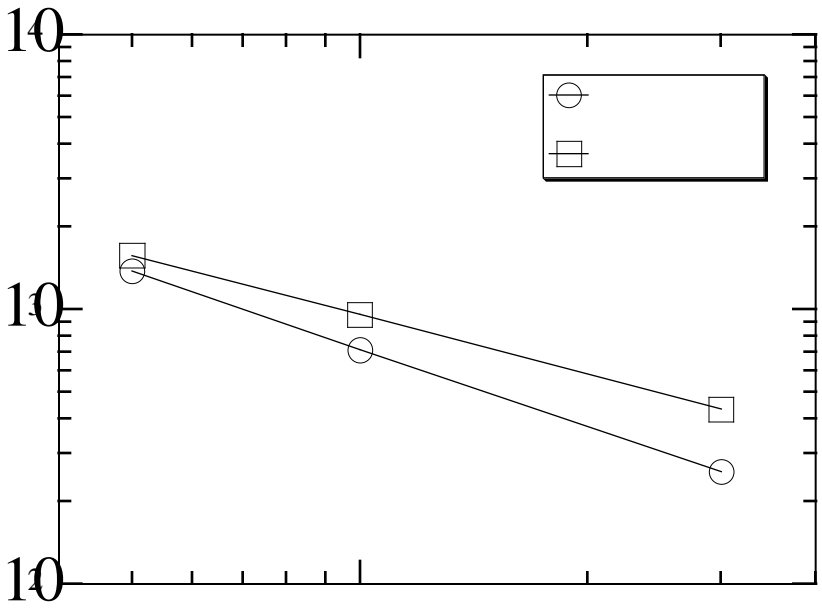

PostScript error Figure 3.13 Effect of silicon implant energy on <D>/D* for the 800ßC anneals.

boron marker layer increases slightly with increasing implant energy for implant doses above the amorphization threshold.

3.4.3.3 Time-Dependence

As shown in Figure 3.10 and Figure 3.11, for short anneal times (30 minutes and 120 minutes at 750ßC and 30 minutes at 800ßC), the time-dependence of the enhanced diffusion for implant doses above the amorphization threshold is the same as the enhanced diffusion for implant doses below the amorphization threshold. However, for long-time anneals (210 minutes and 510 minutes at 750ßC and 120 minutes at 800ßC), the enhancements for high-dose implants are slightly lower than for low-dose implants. This cannot be accounted for simply by assuming the damage in the amorphous region disappears upon recrystallization. If we take the as-implanted silicon profile as a first-order approximation to the initial interstitial concentration after the implant, a significant percentage of the implanted profile can be beyond the amorphous region. Even assuming

that the excess interstitials in the amorphous layer instantaneously recombine during amorphous layer regrowth, a large interstitial supersaturation still remains in the tail region of the implant. For example, Figure 3.14 compares the profiles of $1x10^{14}$ cm^{-2} and

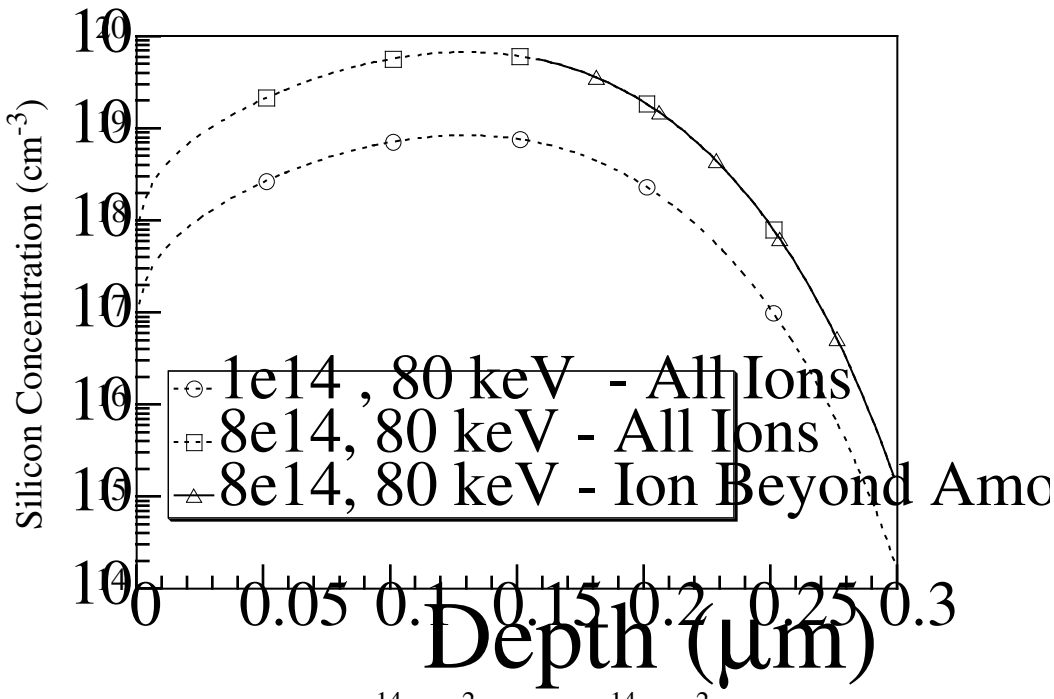

Figure 3.14 Profiles for the $1x10^{14}$ cm^{-2} and $8x10^{14}$ cm^{-2}, 80 keV silicon implants calculated using a Boltzmann Transport Equation solver [27],[28]. The integrated dose beyond the amorphous layer for the $8x10^{14}$ cm^{-2} implant is still $1.9x10^{14}$ cm^{-2}.

$8x10^{14}$ cm^{-2}, 80 keV silicon implants calculated using a Boltzmann Transport Equation (BTE) solver [27],[28]. Using the amorphous layer depth measured by RBS, the figure shows that the integrated dose beyond the amorphous layer is $1.9x10^{14}$ cm^{-2} for the $8x10^{14}$ cm^{-2} silicon implant which is still a larger dose than the $1x10^{14}$ cm^{-2} silicon implant. There must be an additional sink for interstitials which reduces the interstitial concentration much faster for the amorphizing implant. As already shown in Chapter 2, extended defects which form at amorphous silicon/crystalline silicon interfaces are effective gettering sites for interstitials. These extended defects are the most likely candidate for removing the excess silicon interstitials for amorphizing implants such that

for long anneal times, the enhancements are lower compared to sub-amorphization implants.

3.4.3.4 Temperature-Dependence

Figure 3.15 shows the temperature-dependence of the enhanced diffusion for high-

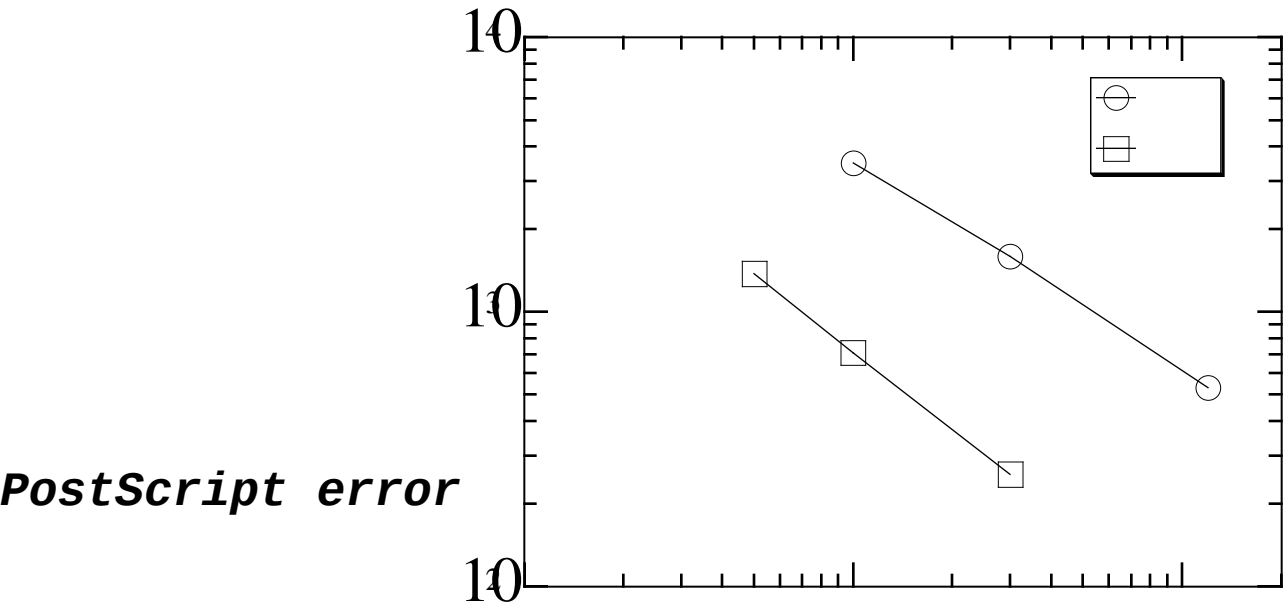

Figure 3.15 Enhancements in boron diffusivity for identical high-dose silicon implants ($4x10^{15}$ cm^{-2}, 50 keV) annealed at 750ßC and 800ßC.

dose implants. In agreement with previous work, the enhancements are larger and last longer for the lower temperature. The result of these two combined effects is that the final doping profile can be broader for samples annealed at lower temperatures as previously pointed out by Packan [11].

3.4.3.5 Dependence on Marker Layer Dose

Figure 3.16 and Figure 3.17 directly compare some of our data to data from Packan [11] for anneals at 750ßC and 800ßC, respectively. The enhancements we measured are

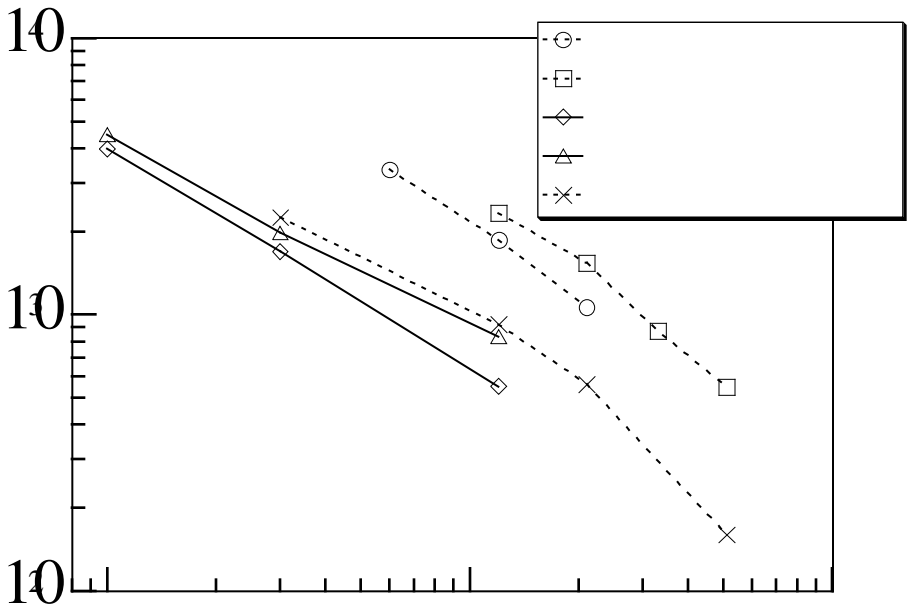

PostScript error Figure 3.16 Comparison of low-dose enhancements from [11] versus the high-dose enhancements from this study after 750ßC furnace annealing. The dotted lines represent data for sub-amorphizing implants and the solid lines represent data for amorphizing implants.

consistently lower than those measured by Packan, even for identical implant doses and energies. The explanation for this behavior is that the enhanced diffusion is also a function of the boron marker layer dose as recently verified by Griffin *et al.* [56]. In their experiment, the enhanced diffusion for a higher-dose marker layer was less than for a lower-dose marker layer for identical silicon damage implants. Packan s marker layers were $7x10^{11}$ cm^{-2} implanted layers with peak boron concentrations close to $1x10^{16}$ cm^{-3} while our epitaxially grown layers had doses between 1 and $3x10^{13}$ cm^{-2} and peak concentrations around $1x10^{18}$ cm^{-3}. The lower enhancements observed for our higher-dose marker layers as compared to Packan s lower-dose marker layers is consistent with Griffin s result.

This dependence of enhanced diffusion on marker layer dose has been modeled in [60] via a boron clustering reaction:

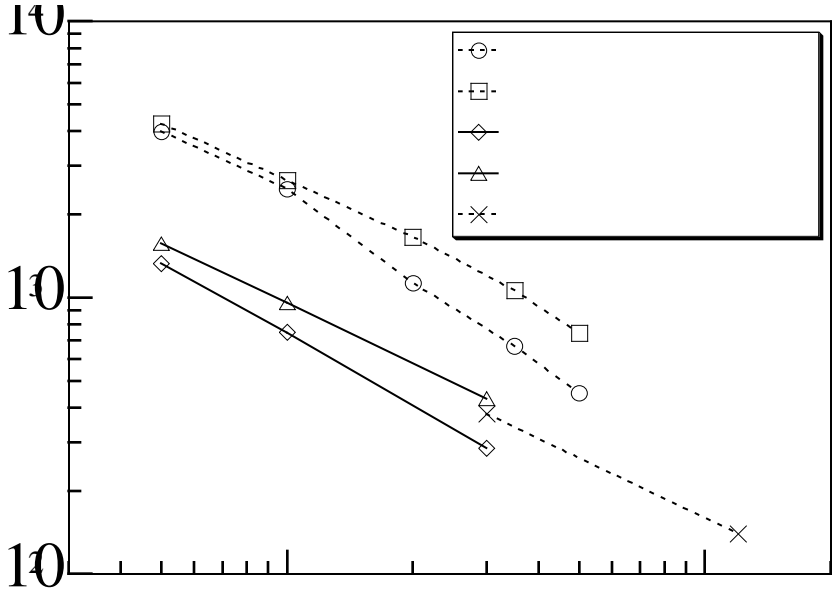

Figure 3.17 Comparison of low-dose enhancements from [11] versus the high-dose enhancements from this study after 800ßC furnace annealing. The dotted lines represent data for sub-amorphizing implants and the solid lines represent data for amorphizing implants.

PostScript

$$B_S + B_I \Leftrightarrow BB_{cl} \tag{3.1}$$

where B_S represents a stationary substitutional boron atom, B_I represents a mobile boron/interstitial pair, and BB_{cl} represents a nonmobile two atom boron cluster. For higher-dose marker layers and the same implant damage, more boron becomes paired with interstitials via the pairing reaction:

$$B_S + I \Leftrightarrow B_I \tag{3.2}$$

The larger B_I concentration drives the reaction in Eq. 3.1 to the right resulting in more clustered, immobile boron for higher-dose marker layers and less overall enhanced diffusion as compared to a lower-dose marker layer. This model can be verified simply by measuring the electrically active boron concentration for different marker layer doses.

Higher-dose marker layers should have a lower percentage of electrical activation if the boron clusters are inactive.

3.4.3.6 RTA Compared to Furnace Anneals

In Figure 3.8, the 745ßC, 2 minute RTA sample does not show any obvious deviation from the 750ßC furnace annealed samples. The RTA sample lies within the extrapolated range for a sample furnace annealed at 750ßC for 2 minutes suggesting there is no substantial difference between an RTA and a furnace anneal for this condition.

3.5 Measurement of Inert Diffusivity

Inert diffusion coefficients in Czochralski (CZ) silicon have been shown to vary depending on oxygen content [61]. Oxygen precipitate (SiO_2) formation requires additional volume which can be provided via the emission of silicon interstitials or the absorption of silicon vacancies. This interaction between oxygen precipitation and point defect concentrations causes variations in the inert diffusivity. However, in float-zone (FZ) silicon, the oxygen content is low enough that oxygen precipitation is negligible, and so for more reliable measurements of inert diffusion coefficients, FZ silicon is typically used. In this section we investigate the crystal quality of the epitaxial silicon layers we have used in our experiments. We have performed a careful study to compare the inert boron diffusion coefficients in epitaxially grown silicon and float-zone (FZ) silicon.

3.5.1 Experimental Procedure

Two sets of wafers were used in this experiment. The starting material for the first set of wafers was 4-inch 5-10 Ω-cm CZ, <100>, n-type silicon. Low-pressure (60 mtorr), low-temperature (800ßC) silicon epitaxy via the decomposition of dichlorosilane (SiH_2Cl_2) was used to grow boron marker layers approximately 2000 thick with peak concentrations around $1x10^{18}$ cm^{-3}. Epitaxial growth was continued for another 4000 to grow lightly-doped arsenic buffer layers on top of the boron marker layer. Diborane (B_2H_6) and arsine (AsH_3) were the source gases for boron and arsenic, respectively,

during the epitaxy growth. These conditions are representative of the epitaxial silicon layers grown for the experiments presented earlier in this chapter and the experiments presented in Chapter 2. After epitaxial growth, low pressure chemical vapor deposition (LPCVD) was used to deposit first a 1300 thick oxide followed by an 800 thick nitride layer. The starting material for the second set of wafers was 3-inch 8-12 Ω-cm FZ, <100>, n-type silicon. A 60 minute dry oxidation at 1000ßC was used to grow a 500 thick screen oxide, then a $2x10^{13}$ cm^{-2}, 160 keV boron implant was done at a tilt angle of 7ß. A 900ßC, 10 minute argon anneal was done to anneal out all the implantation damage and activate the implanted boron. LPCVD was then used to deposit an 800 thick nitride layer.

At this point both the epitaxially grown wafers as well as the FZ wafers contained stable boron doped layers capped on both the front and back sides by oxide/nitride layers. The oxide/nitride layers were utilized to ensure that the true inert boron diffusivities were measured. Hill [62] found that dopant diffusivity was independent of the ambient conditions for an oxide/nitride/oxide capped region. The nitride layer serves as a physical barrier preventing any surface reaction from occurring at the silicon/oxide interface while the oxide layer provides stress-relief between the silicon and the nitride. Stresses caused by nitride directly on silicon have been shown to affect the diffusivity of underlying dopants [63].

Wafers were annealed in pairs, one epitaxially-grown wafer along with one FZ wafer, to ensure identical thermal treatments. An 800ßC anneal for 112 hours and an 850ßC anneal for 48 hours were done in argon ambients. After annealing, nitride layers were etched in hot phosphoric acid and oxide layers were stripped in buffered HF. Boron profiles in all the samples were obtained via SIMS analysis using an oxygen primary beam in a Cameca IMS-3f system. Initial boron profiles were obtained from samples processed as described above except that no final anneal was performed.

3.5.2 Results

Due to either variations in the boron epilayer growth or error in the SIMS data, some of the SIMS profiles had to be translated in order for the boron peaks of the annealed

samples to coincide with the initial profiles. However, in no case did the translation require more than a 200 shift in either direction which is very small compared to the total depth of analysis which was greater than 9000 (0.9 µm) for all samples. The initial profiles were diffused into the final profiles using SUPREM-IV by scaling the default boron diffusion coefficient up or down by constant multiplicative factors. The best-fit diffusivities were obtained by minimization of the least-squares error of a point-by-point comparison of the SIMS data to the simulated boron profile. For the FZ samples, the optimization was done for data points beyond 0.2 µm due to anomalous humps in the boron profiles at the surface (see Figure 3.20 and Figure 3.21).

The SIMS data for the epitaxially grown boron marker layers annealed at 800ßC and 850ßC are shown in Figure 3.18 and Figure 3.19, respectively, along with the optimized

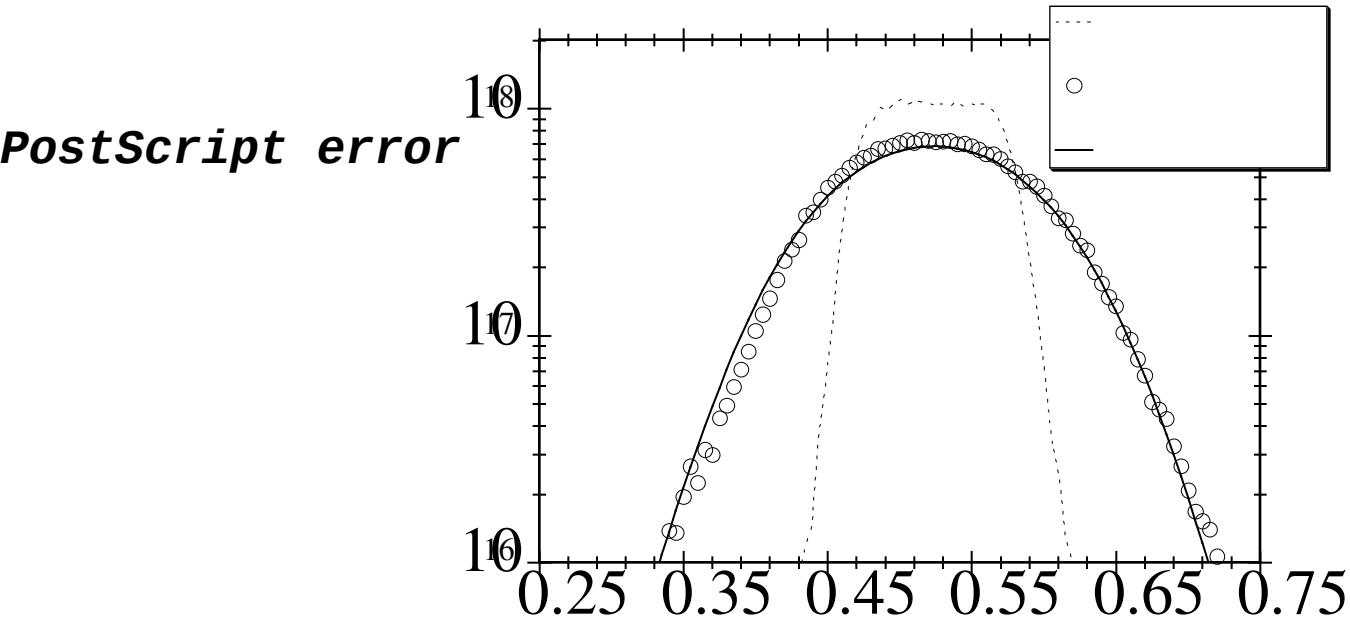

Figure 3.18 Comparison of SIMS data and optimized SUPREM-IV simulation for the epitaxially grown boron marker layer annealed at 800ßC for 112 hours. For the optimized SUPREM-IV simulation, D_B^* was scaled by 0.81X.

SUPREM-IV simulations. SIMS data for the FZ silicon material annealed at 800ßC and 850ßC are shown in Figure 3.20 and Figure 3.21, respectively, again along with optimized SUPREM-IV simulations. Table 3.3 gives the scaling factors required to match the data. In

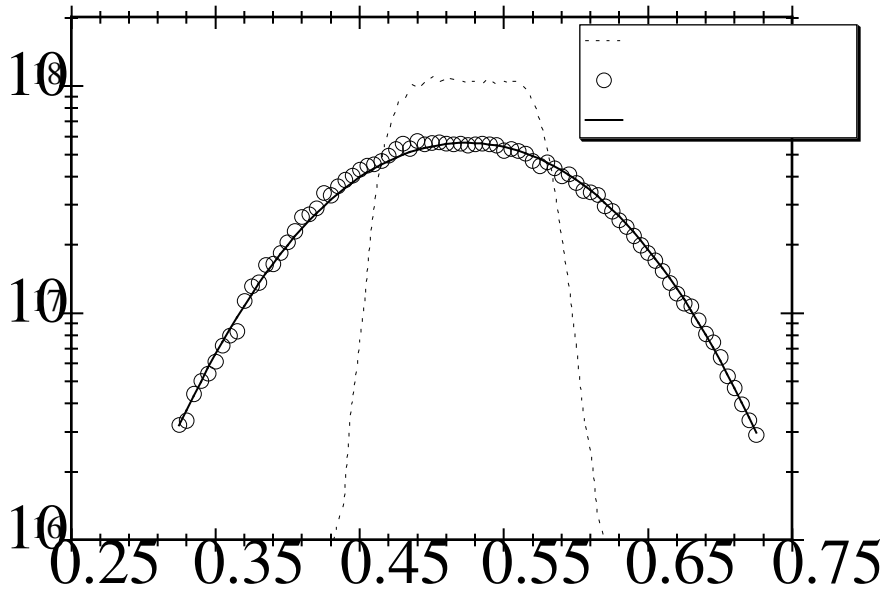

Figure 3.19 Comparison of SIMS data and optimized SUPREM-IV simulation for the epitaxially grown boron marker layer annealed at 850ßC for 48 hours. For the optimized SUPREM-IV simulation, D_B^* was scaled by 0.66X.

PostScript error

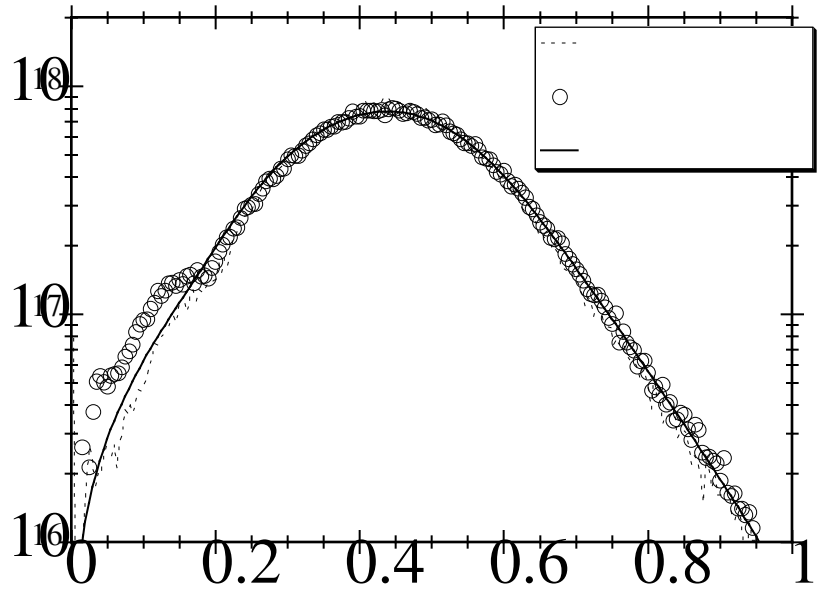

Figure 3.20 Comparison of SIMS data and optimized SUPREM-IV simulation in FZ material annealed at 800ßC for 112 hours. For the optimized SUPREM-IV simulation, D_B^* was scaled by 0.71X.

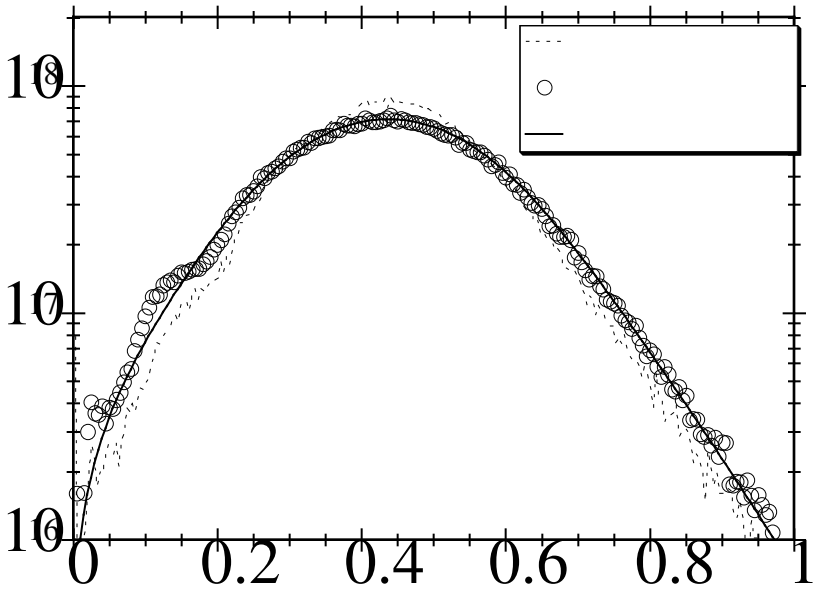

Figure 3.21 Comparison of SIMS data and optimized SUPREM-IV simulation in FZ material annealed at 850ßC for 48 hours. For the optimized SUPREM-IV simulation, D_B^* was scaled by 0.73X.

PostScript error

Anneal Temp. (ßC)	Anneal time (hours)	D^*_{epi}/D^* (unitless)	D^*_{FZ}/D^* (unitless)	D^*_{epi}/D^*_{FZ} (unitless)
800	112	0.81	0.71	1.1
850	48	0.66	0.73	0.90

Table 3.3 Scaling factors for extracted inert boron diffusivities in epitaxially grown silicon and FZ silicon. D^*_{epi} is the inert diffusivity in the epi material, D^*_{FZ} is the inert diffusivity in FZ material, and D^* is the default boron diffusivity in SUPREM-IV [7].

all cases, the inert diffusion coefficient is within 40% of the default value given in SUPREM-IV. At most this translates into a scaling up or down of all the enhanced diffusivities extracted in previous sections. The final column in the table gives the ratio of the scale factor in epitaxially grown material to the scale factor in FZ material. The inert diffusion coefficients in the two materials agree quite well which indicates that the quality of the epitaxial material is comparable to the FZ material, at least with respect to oxygen content.

However, just because the inert diffusivities are nearly identical does not guarantee that the two materials behave the same under all conditions. For example van Oostrum *et al*. [64] have measured different diffusion behavior in three types of epitaxy material, low-temperature chemical vapor deposition (CVD), molecular beam epitaxy (MBE), and fast gas switching CVD. Of the three growth mechanisms, the low-temperature CVD is closest to our epitaxially grown material. Multiple boron spikes were grown using the three techniques, then the samples were thermally oxidized and the oxidation-enhanced diffusion (OED) of the boron spikes was measured using SIMS. For the MBE and fast gas switching CVD material, the amount of OED decreased for boron spikes farther from the growing interface. In contrast, for the low-temperature CVD material, the OED was the same for all boron spikes. van Oostrum explained this result by postulating that large numbers of grown-in vacancy defects were present in the MBE and fast gas switching CVD materials but not the higher-quality low-temperature CVD material. During oxidation in the MBE and fast gas switching CVD samples, the injected interstitial concentration decreased significantly as a function of depth due to recombination with the grown-in vacancy defects. In order to further ensure that our epitaxial material is comparable in crystal quality to FZ material, we would have to perform the same experiment as van Oostrum. Although this experiment has not been done, the normal boron OED measured in our epitaxy material for the 900ßC, 2 hour wet oxidation (see Section 2.2.2) agrees with Packan s measurement of boron OED in FZ material [11].

3.6 Summary

In this chapter, we reviewed the recent literature on the effects of implantation damage on dopant diffusion. Until now, there has been no experimental work that addresses just the effect of implantation damage above the amorphization threshold on dopant diffusion. Previous work has addressed either implantation damage below the amorphization threshold or implantation damage above the amorphization threshold in conjunction with high concentration diffusion, dopant precipitation and clustering, and interactions between the regrowth of the amorphous layer and the dopant. Using silicon epitaxy, we have

fabricated test structures which eliminate these factors and addresses only the issue of IED as a function of implant dose, below and above the amorphization threshold.

Surprisingly, for short anneal times, the enhanced diffusion of a boron marker layer is not a function of the implant damage dose, even as the amorphization threshold is crossed. However, for long anneal times, the enhancements for amorphizing implants are somewhat less than the enhancements for sub-amorphizng implants. This behavior is attributed to the extended defects created by amorphizing implants which have been shown in Chapter 2 to reduce interstitial concentrations during OED and IED. Similar to experimental results for low-dose implants, the enhancement does increase with increasing damage implant energy and the enhancements are larger and last longer at lower temperatures. The enhanced diffusion has also been found to be a function of marker layer dose with higher-dose marker layers exhibiting lower enhancements for identical damage implants. Finally, an RTA annealed sample did not show any obvious difference from the extrapolation of furnace-annealed samples.

An experiment to determine the inert boron diffusion coefficients in epitaxially grown material versus FZ material was also performed. For 800ßC and 850ßC anneals in an argon ambient, the inert diffusivities in both materials were within 40% of the default value given in SUPREM-IV. More important, the inert boron diffusion coefficient in the epitaxial material was almost identical to the inert diffusion coefficient in FZ material indicating that the epitaxial material is comparable in crystal quality to the FZ material with respect to oxygen content.

FrameMaker has detected one or more PostScript errors in this document.
()
Please check your output.